Journal of Power Sources 196 (2011) 8531–8538

Contents lists available at ScienceDirect

Journal of Power Sources

journal homepage: www.elsevier.com/locate/jpowsour

High performance ceramic interconnect material for solid oxide fuel cells (SOFCs): Ca- and transition metal-doped yttrium chromite

Kyung Joong Yoon*, Jeffrey W. Stevenson, Olga A. Marina

Pacific Northwest National Laboratory, P.O. Box 999, Richland, WA 99352, USA

ARTICLE INFO

Article history:
Received 7 June 2011
Received in revised form 23 June 2011
Accepted 24 June 2011
Available online 2 July 2011

Keywords:
Doped yttrium chromite
SOFC interconnect
Sintering
Chemical expansion
Electrical conductivity

ABSTRACT

The effect of transition metal substitution on thermal and electrical properties of Ca-doped yttrium chromite was investigated in relation to use as a ceramic interconnect in high temperature solid oxide fuel cells (SOFCs). 10 at.% Co, 4 at.% Ni, and 1 at.% Cu substitution on B-site of 20 at.% Ca-doped yttrium chromite led to a close match of thermal expansion coefficient (TEC) with that of 8 mol% yttria-stabilized zirconia (YSZ), and a single phase $Y_{0.8}Ca_{0.2}Cr_{0.85}Co_{0.1}Ni_{0.04}Cu_{0.01}O_3$ remained stable between 25 and 1100 °C over a wide oxygen partial pressure range. Doping with Cu significantly facilitated densification of yttrium chromite. Ni dopant improved both electrical conductivity and dimensional stability in reducing environments, likely through diminishing the oxygen vacancy formation. Substitution with Co substantially enhanced electrical conductivity in oxidizing atmosphere, which was attributed to an increase in charge carrier density and hopping mobility. Electrical conductivity of $Y_{0.8}Ca_{0.2}Cr_{0.85}Co_{0.1}Ni_{0.04}Cu_{0.01}O_3$ at 900 °C is 57 S cm^{-1} in air and 11 S cm^{-1} in fuel ($pO_2 = 5 \times 10^{-17}$ atm) environments. Chemical compatibility of doped yttrium chromite with other cell components was verified at the processing temperatures. Based on the chemical and dimensional stability, sinterability, and thermal and electrical properties, $Y_{0.8}Ca_{0.2}Cr_{0.85}Co_{0.1}Ni_{0.04}Cu_{0.01}O_3$ is suggested as a promising SOFC ceramic interconnect to potentially overcome technical limitations of conventional acceptor-doped lanthanum chromites.

1. Introduction

A solid oxide fuel cell (SOFC) has been considered as an attractive power generation system due to its high efficiency, low pollution, multi-fuel flexibility, and modularity. In SOFC stacks, multiple cells are connected in series to obtain the desired voltage output for practical applications. The interconnect is placed between individual cells to provide electrical connection between the anode of one cell to the cathode of the other, and to physically separate the fuel gas from the oxidant. Thus, the interconnect is exposed to a large oxygen chemical potential gradient at high temperatures, which imposes strict requirements in materials properties. There are two different approaches for SOFC interconnects [1,2]. Metallic interconnects are commonly used in anode-supported planar SOFC designs for intermediate temperature operations because of their high electrical and thermal conductivity, low cost, and good workability [3,4]. The application of metallic interconnects is limited to temperatures below ~800 °C due to the oxide scale growth and Cr evaporation at higher temperatures in oxidizing environments [5–8]. For SOFC stack designs which utilize higher operating temperatures, ceramic interconnects are required. Currently, acceptor-doped lanthanum chromite is the predominant ceramic interconnect material [2,9]. Stoichiometric lanthanum chromite is stable under SOFC operating conditions, but exhibits poor electrical conductivity and extremely inferior sintering behavior [9]. Electrical conductivity of lanthanum chromite is improved by doping with alkaline earth metals (Ca and Sr) which act as electron acceptors on the trivalent lanthanum site [10–15]. Substitution of alkaline earth metal also enhances the sinterability [16,17]. It has been observed that Ca-substituted specimens can be sintered at lower temperatures than Sr-substituted ones [18], and thermodynamic calculations predicted that Ca-doping should reduce CrO_3 vapor pressure and prevent the formation of a Cr_2O_3 layer without La_2O_3 precipitation [19]. However, heavy Ca-doping reduces chemical and dimensional stability in reducing environments, causing decomposition of the perovskite structure in fuel conditions [20] as well as internal stress and deformation under large oxygen partial pressure gradients due to chemical expansion [21]. Sintering behavior of acceptor-doped lanthanum chromite is strongly influenced by the A to B ratio in the ABO_3 structure, and A-site excess Ca-doped lanthanum chromites could be sintered to over 95% of theoretical density at 1300 °C [16,22]. However, excess A-site elements tend to react with the zirconia electrolyte during sintering to produce undesirable secondary phases such

* Corresponding author at: Pacific Northwest National Laboratory, 902 Battelle Blvd, Richland, WA 99352, USA. Tel.: +1 509 372 4255; fax: +1 509 375 2186.
E-mail addresses: kyungjoong.yoon@pnnl.gov, kyungjoong.yoon@gmail.com (K.J. Yoon).

0378-7753/$ – see front matter © 2011 Elsevier B.V. All rights reserved.
doi:10.1016/j.jpowsour.2011.06.089

as $La_2Zr_2O_7$ and $CaZrO_3$ [23,24]. To lower the sintering temperature of acceptor-doped lanthanum chromite, various synthesis and fabrication techniques have been proposed such as the use of highly reactive powders [25–28], sintering in reducing environments [28,29], and sintering between chromium oxide plates with fast heating and cooling rates [30]. However, these measures increase fabrication complexity and manufacturing costs, and only lower the sintering temperature by 100–200 °C, which is still inadequate. In addition, lanthanum chromite is susceptible to hydration in moist environments, and the volume expansion on a formation of lanthanum hydroxide ($La(OH)_3$) causes disintegration of the chromite structures [31,32]. Also, doped lanthanum chromites undergo a phase transition from orthorhombic to rhombohedral symmetry upon heating, which causes loss of mechanical strength [33]. Therefore, an alternate interconnect material is needed to overcome these technical limitations of acceptor-doped lanthanum chromite.

Yttrium chromite-based perovskites exhibit several attractive features for interconnect applications over lanthanum chromites such as stability with respect to formation of hydroxides [34], low chemical expansion in reducing environments resulting from a "clamping" effect of small unit cells [34], and chemical compatibility with YSZ electrolyte due to the absence of lanthanum [35]. The electrical conductivity of yttrium chromite is known to be relatively low [9], but can be improved by multiple doping on A- and B-sites [36,37]. Electrical and thermal properties of yttrium chromites are strongly influenced by transition metal doping on B-site [38], and the basic properties of yttrium chromite could possibly be refined and optimized by a wide variety of dopants to satisfy the rigorous requirements for SOFC interconnect applications. In this work, yttrium chromites doped with 20 at.% Ca on A-site and various transition metal elements on B-site were synthesized using the glycine nitrate method. The effect of Co-, Ni-, and Cu-doping on thermal and electrical properties of yttrium chromite was investigated, and the optimized composition for SOFC interconnect application was proposed.

2. Experimental

The powders of yttrium chromites doped with 20 at.% Ca on A-site and various transition metal elements on B-site were synthesized using the glycine nitrate process [39]. The standardized precursors of yttrium, calcium, chromium, cobalt, nickel, and copper nitrates were mixed with glycine according to the desired stoichiometric ratio and combusted. The resulting powders were calcined at 1200 °C for 2 h in air. After calcination, the phase purity was verified using an X-ray diffraction (XRD) analysis (Philips 3100 XRG, Philips Analytical Inc.). The phase stability up to 1100 °C was investigated using a Philips X'Pert-MPD X-ray diffractometer with secondary beam graphite monochromated Cu Kα radiation, equipped with an Anton Paar HTK1200 high-temperature chamber. Lattice parameters were obtained by Rietveld refinement using TOPAS software (Bruker AXS) carried out with an orthorhombic structure. The chemical stability in reducing atmosphere was examined by XRD after annealing the powders at 900 °C in humidified hydrogen ($pO_2 = 4.7 \times 10^{-20}$ atm) for 24 h.

Rectangular specimens were prepared by uniaxial pressing at 35 MPa followed by isostatic pressing at 200 MPa. Sintering shrinkages were measured in a dilatometer using 3 mm × 3 mm × 14 mm bars up to 1400 °C. The relative density after sintering at 1300 °C was determined using the Archimedes method, and the samples for scanning electron microscopy (SEM) analysis (JEOL JSM-7600F) were prepared by sintering at 1300 °C for 4 h and thermally etching at 1275 °C. The sintered samples were used to measure thermal expansion coefficients (TECs) in the temperature range of 25–900 °C in air. Isothermal "chemical" expansions were measured in a controlled-atmosphere dilatometer at 900 °C while varying oxygen partial pressure by mixing oxygen and nitrogen for oxidizing atmospheres ($pO_2 = 0.001$–0.21 atm), and carbon dioxide and forming gas (3% H_2 in N_2) for reducing atmospheres ($pO_2 = 5 \times 10^{-17}$–10^{-11} atm). The samples were equilibrated for more than 24 h under specific environment, and the equilibration was confirmed by the stable measured values. Transient thermogravimetric analysis (TGA) was performed on a Mettler Toledo TGA/DSC STAR System Analyzer using ~100 mg of powder samples. The samples were heated up to 900 °C at a ramping rate of 10 °C min^{-1} with 20 ml min^{-1} of air flow, and after the weight of the sample reached a steady-state value, the atmosphere was cycled between oxidizing and reducing environments by repeatedly alternating the supply of air and forming gas (3% H_2 in N_2). The relative weight changes were measured and corrected for buoyancy effects by subtracting data performed on inert material of the same mass as the samples.

Electrical conductivity measurements were performed by a four-probe DC method using 3 mm × 3 mm × 30 mm dense rectangular bars. The electrical contacts were made using Pt wires and Pt paste, and conductivity was measured in the temperature range 600–900 °C in air. Electrical conductivity was also measured as a function of oxygen partial pressure at 900 °C by varying the oxygen partial pressure from 1.0 to 5×10^{-17} atm as described above. Chemical compatibility of doped yttrium chromite with other cell components was investigated by mixing doped yttrium chromite powders with 8 mol% YSZ, NiO, and $(La_{0.8}Sr_{0.2})_{0.95}MnO_3$ (LSM) powders in a 50:50 weight ratio separately, ball-milling for 24 h and firing in air at 1400, 1400, and 1200 °C, respectively, for 12 h. The resulting specimens were crushed and the powders were analyzed by XRD.

3. Results and discussion

3.1. Crystal structure and chemical stability

Fig. 1(a) shows XRD patterns of $Y_{0.8}Ca_{0.2}Cr_{0.85}Co_{0.1}Ni_{0.04}Cu_{0.01}O_3$ powders after calcination at 1200 °C in air and after exposure to reducing environment ($pO_2 = 4.7 \times 10^{-20}$ atm) at 900 °C for 24 h. All the peaks were indexed to the single phase orthorhombic perovskite structure with space group *Pbnm* (62), and no impurity phase was observed. Solubility limit of cobalt in yttrium chromite is higher than 30 at.% [36], and yttrium chromite forms a single phase with up to 15 at.% Ni [37] and 10 at.% Cu [38]. Therefore, precipitation of the dopants was not observed in this composition. After reduction, no phase segregation or decomposition product was found. Moreover, the phase analysis performed *in situ* using high temperature XRD while heating the calcined powder up to 1100 °C in air confirmed the single orthorhombic phase in Fig. 1(b). Therefore, the doped yttrium chromite is chemically stable under the SOFC operating conditions, which differs from the conventional lanthanum chromite. Stoichiometric and acceptor-doped lanthanum chromites typically experience first order phase transition from orthorhombic to rhombohedral symmetry at 250–300 °C upon heating [40–45], which causes volume shrinkage primarily due to shrinking of the CrO_6 octahedral, and subsequent loss of mechanical strength [33,46]. Therefore, improved mechanical reliability is expected for doped yttrium chromite interconnects during start-up and thermal cycles of SOFC stacks due to the absence of phase transformation.

The thermal evolution of selected XRD peaks between 32 and 35 degree is illustrated in Fig. 1(b), and the variation of unit cell parameters with temperature is given in Fig. 2. The shift in peak positions toward lower angle with increasing temperature indicates the

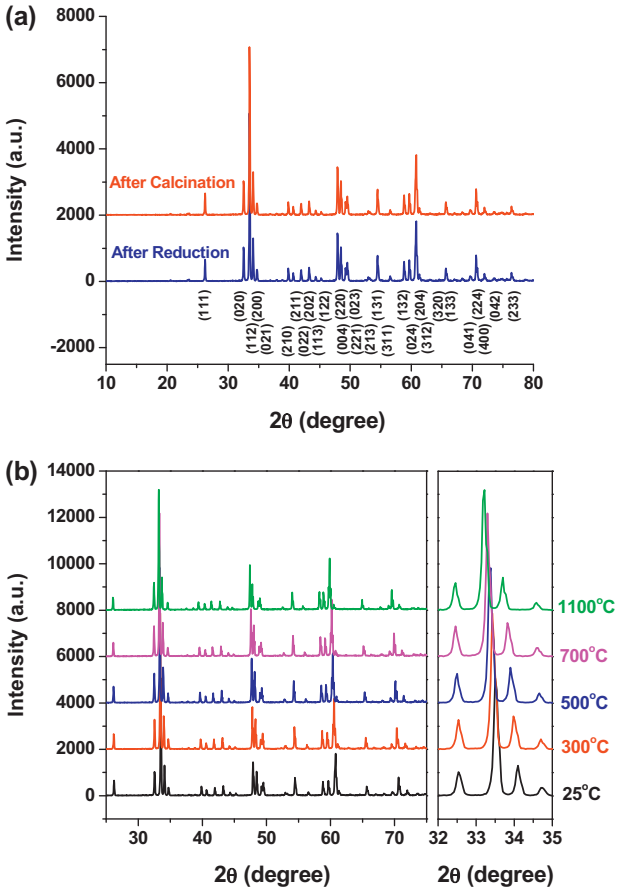

Fig. 1. (a) XRD patterns of $Y_{0.8}Ca_{0.2}Cr_{0.85}Co_{0.1}Ni_{0.04}Cu_{0.01}O_3$ after calcinations in air and after reduction in humidified H_2 at 900 °C for 24 h, and (b) high temperature XRD patterns of the same composition between 25 and 1100 °C in air.

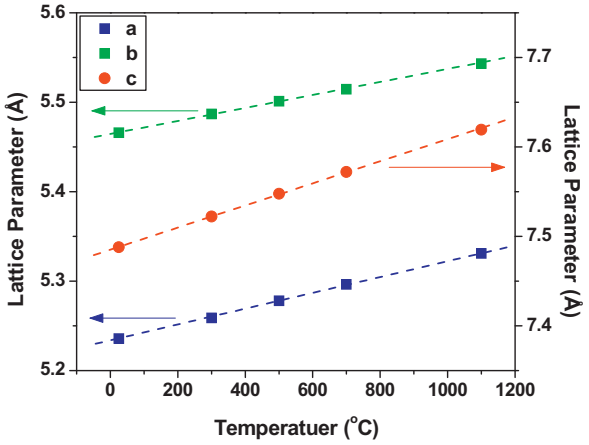

Fig. 2. Variation of lattice parameters of $Y_{0.8}Ca_{0.2}Cr_{0.85}Co_{0.1}Ni_{0.04}Cu_{0.01}O_3$ with temperature between 25 and 1100 °C in air.

temperature-induced unit cell expansion. The lattice parameters obtained by Rietveld refinement on orthorhombic structure of $Y_{0.8}Ca_{0.2}Cr_{0.85}Co_{0.1}Ni_{0.04}Cu_{0.01}O_3$ were $a = 5.236$ Å, $b = 5.478$ Å, and $c = 7.488$ Å at room temperature, and increased linearly with temperature. The TEC value can be estimated from the variation of lattice parameters with temperature using the cubic root of the unit cell volume [37,47], and it was calculated to be 11.0×10^{-6} K^{-1} for $Y_{0.8}Ca_{0.2}Cr_{0.85}Co_{0.1}Ni_{0.04}Cu_{0.01}O_3$, which matches well with that of 8 mol% YSZ (10.8×10^{-6} K^{-1} [48,49]). This value was compared to the experimentally measured value from the dilatometry measurements as described in the following section.

3.2. Thermal expansion

Because the SOFC is a solid-state device, it is important for the cell components to have similar thermal expansions in order to minimize the thermal stress during fabrication, startup, thermal cycles, and shutdown. Table 1 shows the TECs of yttrium chromites doped with 20 at.% Ca on A-site and Co, Ni, and Cu on B-site in air in 25–900 °C temperature range. TEC of the $Y_{0.8}Ca_{0.2}CrO_3$ was 9.7×10^{-6} K^{-1}, which is substantially lower than that of 8 mol% YSZ, 10.8×10^{-6} K^{-1} [48,49]. TEC increased with transition metal substitution, and $Y_{0.8}Ca_{0.2}Cr_{0.85}Co_{0.1}Ni_{0.04}Cu_{0.01}O_3$ (11.1×10^{-6} K^{-1}) gave the closest match to 8 mol% YSZ. The obtained value is in a good agreement with the value calculated by high temperature XRD analysis in the previous section. Without B-site doping, the TEC of chromite-based perovskite has been reported to increase with the amount of alkaline earth element on A-site, and typically, more than 30% substitution is required to match TEC of YSZ [9,50]. In particular, TEC of $Y_{0.6}Ca_{0.4}CrO_3$ gave the best match to that of 8 mol% YSZ [17]. However, when the total calcium content exceeds 25%, calcium chromate ($CaCrO_4$) exsolves from the perovskite structure as a secondary phase because of the limited alkaline-earth solubility, and react with YSZ to form $CaZrO_3$ as a reaction product during co-firing process [24,34,51]. In addition, $CaCrO_4$ dissociates into α and β phases of $CaCr_2O_4$ under reducing environments, and causes large volume expansion [34]. The results of this study suggest that thermal expansion of Ca-doped yttrium chromite can be controlled by B-site substitution while keeping the calcium content below the solubility limit and preventing the formation of the undesired phases. In addition, there was no indication of non-linear thermal expansion behavior resulting from the phase transformation within the measured temperature range, which further supports the phase stability observed by high temperature XRD analysis.

3.3. Sintering behavior

Since the interconnect acts as a physical barrier between fuel and oxidant gases in SOFCs, it should be dense to minimize the loss of fuel efficiency resulting from gas cross leakage and direct mixing. One of the major challenges for the lanthanum chromite-based interconnects is their extremely inferior sintering behavior, which is attributed to the evaporation of chromium vapor species (CrO_3) above 1000 °C, followed by the formation of thin chromium oxide layers (Cr_2O_3) at the interparticle necks inhibiting sintering of particles at the initial stages of sintering [2,14,19,48,52].

Fig. 3(a) illustrates the effect of partial substitution of Co, Ni, and Cu for Cr on sintering shrinkage ($\Delta l/l_o$) of $Y_{0.8}Ca_{0.2}CrO_3$. Without B-site doping, the shrinkage began at about 1300 °C, and only 3% of sintering shrinkage was observed at 1400 °C, which is comparable to the sintering behavior of the acceptor-doped lanthanum

Table 1
Thermal expansion coefficients (TEC) of 20 at.% Ca-doped yttrium chromites with various amounts of B-site dopants (Co, Ni, and Cu) obtained by the dilatometry measurements.

B-site dopants (at.%)			TEC (K^{-1})
Co	Ni	Cu	
0	0	0	9.5×10^{-6}
10	0	0	10.7×10^{-6}
0	10	0	10.0×10^{-6}
10	4	1	11.1×10^{-6}
15	4	1	12.5×10^{-6}
10	10	1	11.8×10^{-6}
15	10	1	13.8×10^{-6}

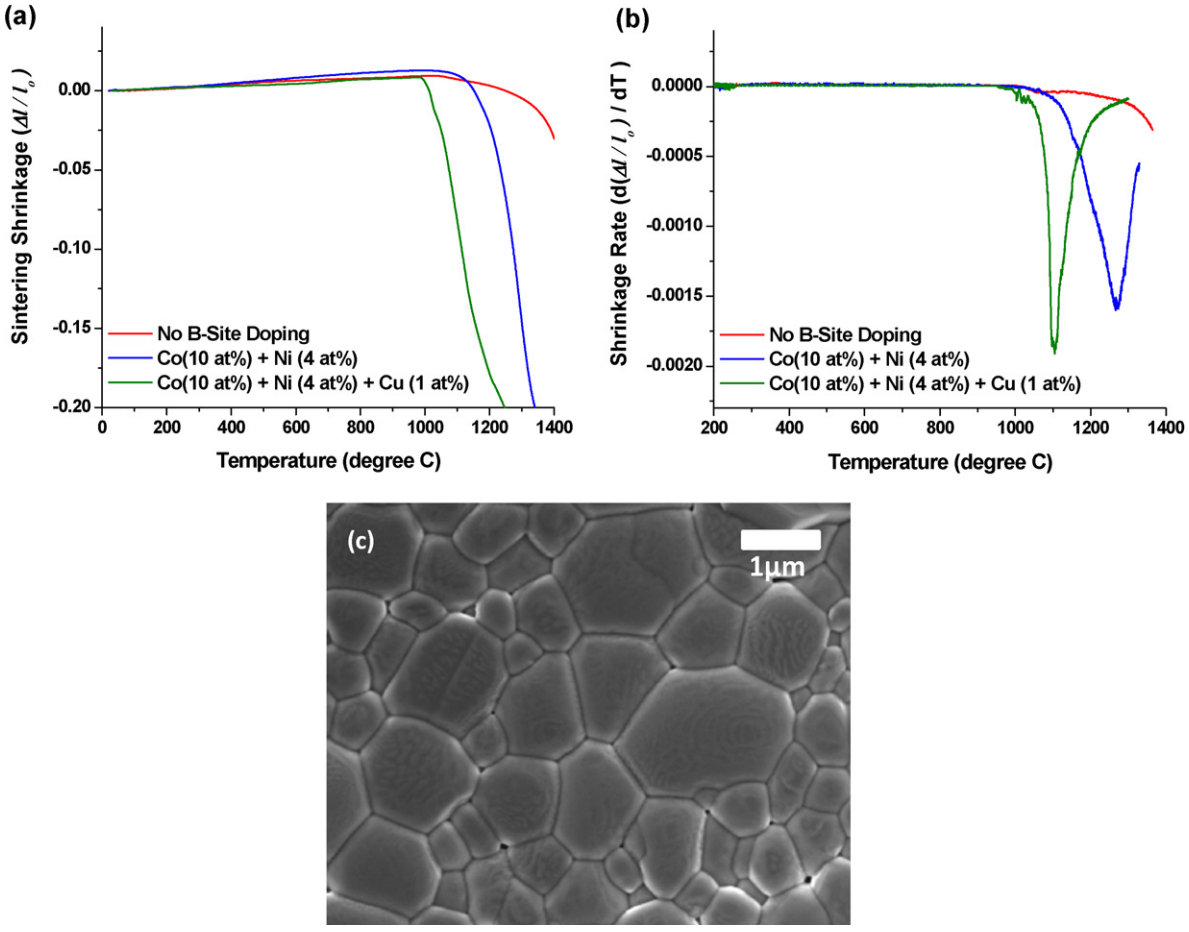

Fig. 3. (a) Linear sintering shrinkage ($\Delta l/l_o$) and (b) shrinkage rate ($d(\Delta l/l_o)/dT$) of $Y_{0.8}Ca_{0.2}CrO_3$, $Y_{0.8}Ca_{0.2}Cr_{0.86}Co_{0.1}Ni_{0.04}O_3$, and $Y_{0.8}Ca_{0.2}Cr_{0.85}Cu_{0.01}Co_{0.1}Ni_{0.04}O_3$ as a function of temperature, and (c) SEM image of $Y_{0.8}Ca_{0.2}Cr_{0.85}Co_{0.1}Ni_{0.04}Cu_{0.01}O_3$ sintered at 1300 °C and thermally etched at 1275 °C.

chromite [15,53]. Sintering curve showed gradual shrinkage over a wide temperature range, which is a characteristic of solid-state sintering [16,53]. With 10 at.% Co and 4 at.% Ni doping on B-site, sintering curve exhibited more rapid shrinkage above 1200 °C, and 20% of sintering shrinkage was observed at 1340 °C. With the addition of 1 at.% Cu, sintering behavior was remarkably improved, showing 20% sintering shrinkage at 1240 °C.

To identify the sintering mechanism and the temperature to achieve a desired (maximum) density, the linear shrinkage rate, $d(\Delta l/l_o)/dT$, was plotted as a function of temperature in Fig. 3(b), in accordance with [54]. As seen in Fig. 3(b), small addition of Cu was highly effective in promoting the densification of yttrium chromite. With the addition of 1 at.% Cu, the maximum shrinkage rate was significantly increased and sintering occurred at much lower temperature. For $Y_{0.8}Ca_{0.2}Cr_{0.85}Co_{0.1}Ni_{0.04}Cu_{0.01}O_3$ the maximum shrinkage took place at 1120 °C, which is about 150 °C lower than the temperature at which the maximum shrinkage of $Y_{0.8}Ca_{0.2}Cr_{0.86}Co_{0.1}Ni_{0.04}O_3$ was observed, 1270 °C. The width of the shrinkage temperature range was also decreased, and the densification process was completed within a narrow temperature range. Such behavior is a typical indication of particle rearrangement process in liquid phase-assisted sintering, where the rapid densification occurs due to the capillary force exerted by the wetting liquid on the solid particles [18,55,56]. Copper is a well known sintering aid and the mechanism is believed to involve the formation of transient liquid phase at relatively low temperatures [55,57–61]. Similarly, the formation of a CuO-rich transient liquid phase could be suggested to occur between 1000 and 1200 °C during the densification of yttrium chromite, and further study is needed to clarify the exact role of Cu in yttrium chromites. In the present work, the amount of Cu was limited to 1 at.% in order to prevent the shape distortion which can possibly occur with excessive amount of liquid phase during liquid phase-assisted sintering [56].

SEM image of $Y_{0.8}Ca_{0.2}Cr_{0.85}Co_{0.1}Ni_{0.04}Cu_{0.01}O_3$ sintered at 1300 °C in Fig. 3(c) shows dense microstructure with small amount of closed pores, which are not gas permeable. The relative density was measured to be ~98% of theoretical density by Archimedes method, which is substantially higher than the acceptable value (~94%) for the ceramic interconnect [27,62]. Thus, it is suggested that adequately dense yttrium chromite-based interconnect can be fabricated by co-firing with other cell components at a processing temperature as low as 1300 °C, and common problems accompanied by high sintering/processing temperatures such as undesired chemical interactions, migration of elements, and excessive sintering of other cell components can be avoided. Further details about chemical compatibility of yttrium chromite with other cell components at the sintering temperature will be discussed in Section 3.6.

3.4. Stability in reducing environment

The volume of chromite-based perovskite materials expands upon reduction due to the loss of lattice oxygen [21,34,63–65]. Two possible mechanisms have been proposed to explain the chemical expansion of chromites. First, the formation of positively charged oxygen vacancies in reducing environments is accompanied by the reduction of Cr^{4+} to Cr^{3+} to maintain the charge neutrality,

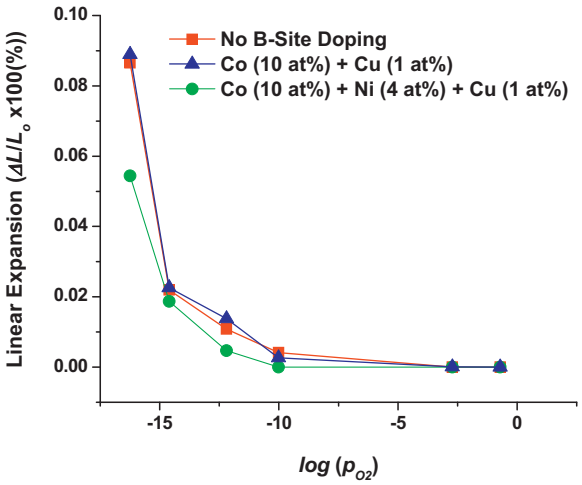

Fig. 4. Isothermal linear expansion of $Y_{0.8}Ca_{0.2}CrO_3$, $Y_{0.8}Ca_{0.2}Cr_{0.89}Co_{0.1}Cu_{0.01}O_3$, and $Y_{0.8}Ca_{0.2}Cr_{0.85}Co_{0.1}Ni_{0.04}Cu_{0.01}O_3$ at 900 °C as a function of oxygen partial pressure.

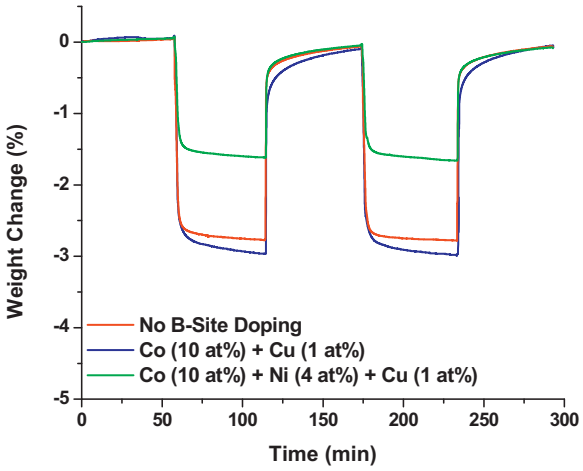

Fig. 5. Isothermal transient TGA curves of $Y_{0.8}Ca_{0.2}CrO_3$, $Y_{0.8}Ca_{0.2}Cr_{0.89}Co_{0.1}Cu_{0.01}O_3$, and $Y_{0.8}Ca_{0.2}Cr_{0.85}Co_{0.1}Ni_{0.04}Cu_{0.01}O_3$ during cycles between air and dry forming gas at 900 °C.

and the increased ionic radius of Cr^{3+} (r_{ion} = 0.615 Å [66]) with respect to Cr^{4+} (r_{ion} = 0.55 Å [66]) may result in the swelling of the chromium-containing oxygen octahedral, which causes the lattice expansion. Another possibility is that the columbic repulsion between cations resulting from the loss of bridging lattice oxygen could cause the rotation of the octahedral to increase their linear distance and lead to a net volume expansion. Fig. 4 shows the effect of B-site dopants on the isothermal chemical expansion of Ca-doped yttrium chromite in the oxygen partial pressure range of 5×10^{-17}–0.21 atm at 900 °C. Expansions in the following were referenced to the initial sample length at 900 °C in air. In all samples no significant expansion was observed until the ambient oxygen partial pressure reached 10^{-10} atm, and the onset of the expansion occurred at $pO_2 = 10^{-12}$ atm. Without B-site doping, $Y_{0.8}Ca_{0.2}CrO_3$ showed the expansion of 0.09% on reduction at $pO_2 = 5 \times 10^{-17}$ atm. Co- and Cu-doped yttrium chromite, $Y_{0.8}Ca_{0.2}Cr_{0.89}Co_{0.1}Cu_{0.01}O_3$, exhibited very similar behavior to $Y_{0.8}Ca_{0.2}CrO_3$. When 4 at.% Ni was added, the isothermal expansion of $Y_{0.8}Ca_{0.2}Cr_{0.85}Co_{0.1}Ni_{0.04}Cu_{0.01}O_3$ decreased to 0.055% under the same condition. Importantly, all samples exhibited good reversibility when cycled between oxidizing and reducing environments, which confirms that no microcracks on internal stress were generated.

Since the SOFC interconnects are exposed to the fuel on one side and the oxidant on the other during the operation, the chemical expansion on the fuel side could cause internal stress and deformation, resulting in the mechanical damage such as the seal failure and the crack formations. In addition, lattice expansion closely correlates with the crack propagation characteristics through the lattice, and decreases toughness and grain strength, potentially leading to transgranular fracture [46]. Therefore, the chemical expansion of chromites could be detrimental to the SOFC stack operation and should be minimized. The chemical expansion of chromite-based materials could be reduced by decreasing the concentration of alkaline earth metal dopant (Ca or Sr) because the low initial concentration of Cr^{4+} allows less oxygen to be removed from the lattice before all of the Cr^{4+} is reduced to Cr^{3+} [34]. However, the charge carriers for electrical conduction in the chromites are electron holes associated with Cr^{4+}, and, thus, the electrical conductivity is also lowered by reducing the concentration of alkaline earth metal dopant. The acceptor-doped yttrium chromite shows the chemical expansion of about 40% less than that of similarly doped lanthanum chromite because the reduced unit cell size of yttrium chromite suppresses the oxygen evolution in reducing atmosphere [34]. The results of the current study indicate that the chemical expansion of the yttrium chromites can be further reduced by Ni substitution on B-site without loss of electrical conductivity.

The chemical expansion is directly related to the defect chemistry and oxygen non-stoichiometry associated with the loss of lattice oxygen and simultaneous reduction of Cr^{4+} to Cr^{3+} [65,67]. To assess the oxygen non-stoichiometry and correlate oxygen evolution with dimensional stability, TGA was performed and the results are shown in Fig. 5. All three compositions of yttrium chromites, $Y_{0.8}Ca_{0.2}CrO_3$, $Y_{0.8}Ca_{0.2}Cr_{0.89}Co_{0.1}Cu_{0.01}O_3$, and $Y_{0.8}Ca_{0.2}Cr_{0.85}Cu_{0.01}Co_{0.1}Ni_{0.04}O_3$, experienced weight changes when cycled between the air and dry forming gas (3% H_2 in N_2) due to the changes in their oxygen nonstoichiometry. In all samples the weight changes were reversible upon cycling, which again indicates the phase stability over the wide oxygen partial pressure range. As seen in Fig. 5, Co- and Cu-doping had almost no effect on the amount of oxygen loss, but Ni-doping remarkably reduced the weight loss on reduction. Thus, Ni substitution for Cr stabilizes the defect structure and suppresses the oxygen evolution in reducing environments, resulting in improved dimensional stability in SOFC operating conditions.

3.5. Electrical conductivity

The electrical conductivity of the interconnect material should be sufficiently high in both oxidizing and reducing environments to minimize the performance loss of SOFC stacks due to the ohmic drop through the interconnect. Despite other superior properties, the yttrium chromites possess lower electrical conductivity than similarly doped lanthanum chromites [9], but doping with alkaline earth metal on A-site and/or transition metal on B-site generally improves the electrical conductivity of chromite-based materials [10,38,68,69]. The effect of Co, Ni, and Cu partial substitution on the electrical conductivity of Ca-doped yttrium chromite in the temperature range between 600 and 900 °C in air is shown in Fig. 6(a). For all compounds, the conductivity increased with temperature as expected for a thermally activated conduction process [10,68–70]. The conductivity increased with Ni doping, but even more so with Co doping. The conductivity values at 900 °C were 10 S cm^{-1} for $Y_{0.8}Ca_{0.2}CrO_3$, 21 S cm^{-1} for $Y_{0.8}Ca_{0.2}Cr_{0.85}Ni_{0.14}Cu_{0.01}O_3$, and 57 S cm^{-1} for $Y_{0.8}Ca_{0.2}Cr_{0.85}Co_{0.1}Ni_{0.04}Cu_{0.01}O_3$. Ni doping increases the electrical conductivity because most of the nickel ions are divalent and act as acceptor dopants in chromite-based oxides [71]. Substi-

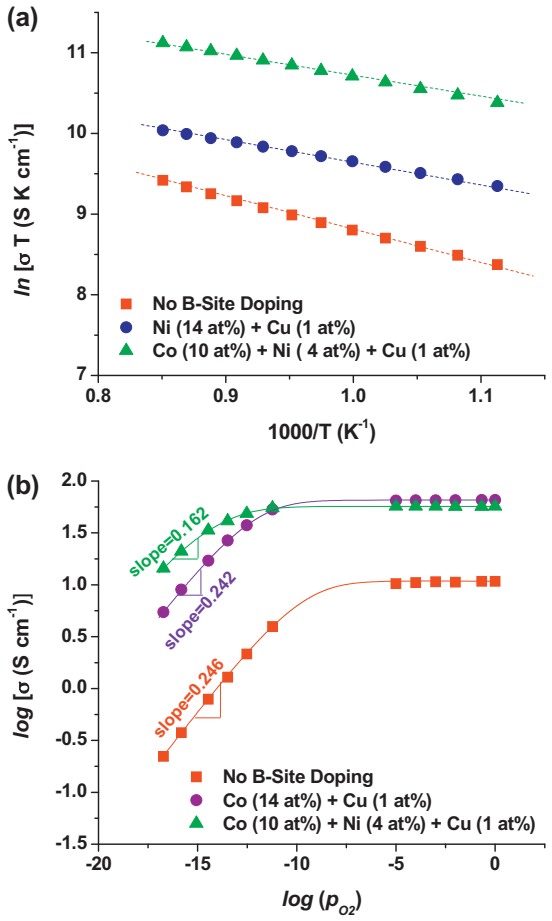

Fig. 6. Plots of (a) $\ln(\sigma T)$ versus $1000/T$ for $Y_{0.8}Ca_{0.2}CrO_3$, $Y_{0.8}Ca_{0.2}Cr_{0.85}Ni_{0.14}Cu_{0.01}O_3$, and $Y_{0.8}Ca_{0.2}Cr_{0.85}Co_{0.1}Ni_{0.04}Cu_{0.01}O_3$ in air, and (b) $\log(\sigma)$ versus $\log(pO_2)$ for $Y_{0.8}Ca_{0.2}CrO_3$, $Y_{0.8}Ca_{0.2}Cr_{0.85}Co_{0.14}Cu_{0.01}O_3$, and $Y_{0.8}Ca_{0.2}Cr_{0.85}Co_{0.1}Ni_{0.04}Cu_{0.01}O_3$ at 900 °C.

tution of Cr with Co likely leads to an increase in both charge carrier density and hopping mobility [36]. Charge carrier population increases due to the disproportionation among the Co sites: Co^{4+} becomes energetically favorable and populated at high temperatures [27,72,73]. Hole mobility also increases because of the low small polaron site energy of Co and rapid electron transfer between Co^{3+} and Co^{4+} [74]. The linear relationship between $\ln(\sigma T)$ and $1/T$ in Fig. 6(a) suggests adiabatic small polaron mechanism, in which the charge carriers are able to jump to an adjacent unoccupied site whenever an atomic displacement favoring the jump occurs [12,74–76]. The activation energies obtained from the slopes of Fig. 6(a) were 0.24 eV $Y_{0.8}Ca_{0.2}CrO_3$, and around 0.15 eV for both $Y_{0.8}Ca_{0.2}Cr_{0.85}Ni_{0.14}Cu_{0.01}O_3$ and $Y_{0.8}Ca_{0.2}Cr_{0.85}Co_{0.1}Ni_{0.04}Cu_{0.01}O_3$. The activation energy values are close to the reported ones [35,68], and decrease of activation energy of chromite-based perovskites with transition metal doping is consistent with previous studies [36,37].

The electrical conductivity of doped yttrium chromites during the oxygen partial pressure change from 1 atm to 5×10^{-17} at 900 °C is given in Fig. 6(b). The conductivities were independent of pO_2 in the high oxygen partial pressure region and decreased below a critical oxygen partial pressure, in agreement with the *p*-type conduction mechanism [37,68]. At high oxygen partial pressure, the charge imbalance caused by doping is compensated by the formation of holes, and the number of charge carriers is determined by the amount of dopants. Thus, the electrical conductivity is independent of oxygen partial pressure when the electronic charge compensation is dominant. Below the critical oxygen partial pressure, lattice oxygen is released to the atmosphere and the loss of oxygen creates positively charged oxygen vacancies that consume positively charged holes to maintain the charge neutrality. Therefore, the conductivity develops strong dependence on oxygen partial pressure and decreases with decreasing pO_2 as the ionic charge compensation becomes important.

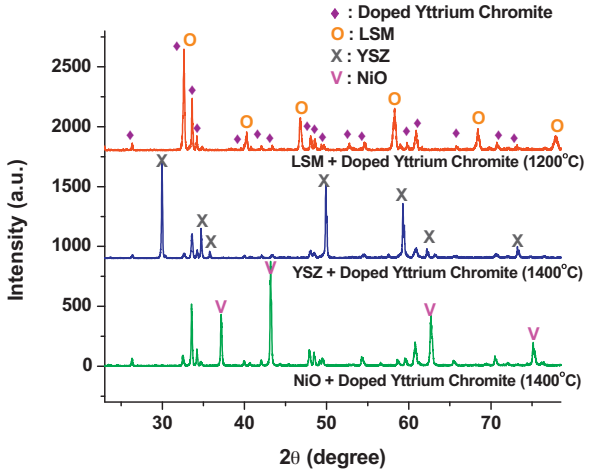

Fig. 7. XRD patterns of mixtures of doped yttrium chromite ($Y_{0.8}Ca_{0.2}Cr_{0.85}Co_{0.1}Ni_{0.04}Cu_{0.01}O_3$) and 8 mol% YSZ (50:50 wt%) fired at 1400 °C, doped yttrium chromite and NiO (50:50 wt%) fired at 1400 °C, and doped yttrium chromite and LSM (50:50 wt%) fired at 1200 °C for 24 h in air.

Also seen in Fig. 6(b), the $Y_{0.8}Ca_{0.2}Cr_{0.85}Co_{0.14}Cu_{0.01}O_3$ showed slightly higher conductivity than $Y_{0.8}Ca_{0.2}Cr_{0.85}Co_{0.1}Ni_{0.04}Cu_{0.01}O_3$ in the oxidizing atmosphere. Since the total amounts of B-site dopants were identical, Co-doping is more effective in increasing the conductivity in oxidizing environment, as suggested above. In reducing environments, the sample containing Ni showed higher electrical conductivity compared to that without Ni. The slopes of the $\log(\sigma)$ versus $\log(pO_2)$ for the sample without B-site dopants and with Co and Cu dopants were close to 0.25 implying a $pO_2{}^{1/4}$ dependence of electrical conductivity, indicating predominant ionic charge compensation and negligible hole concentration [68,75]. The slope for the sample containing Ni was 0.162, which indicates that the system did not reach the extreme reducing conditions and both ionic and electronic compensation mechanisms were operative. On further decrease in pO_2, a 1/4 dependence could be expected. An absolute conductivity value of 11 S cm^{-1} was measured for the $Y_{0.8}Ca_{0.2}Cr_{0.85}Co_{0.1}Ni_{0.04}Cu_{0.01}O_3$ at 900 °C at the partial oxygen pressure of 5×10^{-17} atm. Because the value of 1 S cm^{-1} is a well-accepted minimum conductivity for the interconnect materials to be used in SOFCs [2], the electrical conductivity of $Y_{0.8}Ca_{0.2}Cr_{0.85}Co_{0.1}Ni_{0.04}Cu_{0.01}O_3$ in both oxidizing and reducing environments satisfies this requirement.

3.6. Chemical compatibility

The ceramic interconnects are usually fabricated by co-sintering with other cell components to minimize the interfacial resistance and simplify the manufacturing procedure. During co-sintering process, traditional lanthanum chromite-based materials may chemically interact with other cell components and possibly form undesired secondary phases such as $La_2Zr_2O_7$ [24,77,78], resulting in performance degradation and subsequent cell failure due to increase of resistance and thermal stresses [9]. The use of Ca-doped $YCrO_3$ instead of $LaCrO_3$ would be advantageous in avoiding the $La_2Zr_2O_7$ formation, and reduction of the sintering temperature

through transition metal doping on B-site is likely to further assist in suppressing the undesired reactions.

The chemical compatibility of $Y_{0.8}Ca_{0.2}Cr_{0.85}Co_{0.1}Ni_{0.04}Cu_{0.01}O_3$ with 8 mol% YSZ, NiO, and LSM was evaluated using the XRD analysis. The chromite–YSZ (50:50 wt%) mixture was co-fired in air for 24 h at 1400 °C (above the densification temperatures), and so was the chromite–NiO (50:50 wt%) mixture. The chromite–LSM (50:50 wt%) mixture was co-fired at 1200 °C, the typical cathode sintering temperature. The XRD patterns of these mixtures are given in Fig. 7. All peaks of the composites corresponded to the individual constituents only, and no reaction product was observed. Therefore, detrimental secondary phase formation is not expected between the doped yttrium chromite interconnect and standard cell components under normal processing and operating temperatures.

4. Conclusions

Electrical and thermal properties of Ca-doped yttrium chromite were improved through multiple transition metal doping (Co, Ni, and Cu) on B-site for potential interconnect applications in the SOFCs. Sintering and densification was facilitated by Cu substitution. Co substitution effectively enhanced the electrical conductivity in oxidizing atmosphere and Ni substitution improved stability toward reduction, lowering the chemical expansion and enhancing the electrical conductivity in reducing atmospheres. With optimized amounts of Co, Ni, and Cu dopants, a good match in thermal expansion coefficients with 8 mol% YSZ was achieved. Chemical compatibility of doped yttrium chromite with YSZ, NiO, and LSM was confirmed at the standard cell processing temperatures. Based on the improved stability and thermal and electrical properties, the optimized composition of yttrium chromite, $Y_{0.8}Ca_{0.2}Cr_{0.85}Co_{0.1}Ni_{0.04}Cu_{0.01}O_3$, is recommended for use as a ceramic interconnect material for SOFCs.

Acknowledgements

This work was funded by the U.S. Department of Energy's Solid-State Energy Conversion Alliance (SECA) Core Technology Program. PNNL is operated by Battelle Memorial Institute for the U.S. Department of Energy under Contract DE-AC06-76RLO 1830.

References

[1] S.P.S. Badwal, K. Foger, Ceramics International 22 (1996) 257–265.
[2] W.Z. Zhu, S.C. Deevi, Materials Science and Engineering A 348 (2003) 227–243.
[3] W.Z. Zhu, S.C. Deevi, Materials Research Bulletin 38 (2003) 957–972.
[4] A.B. Stambouli, E. Traversa, Renewable and Sustainable Energy Reviews 6 (2002) 433–455.
[5] Y. Matsuzaki, I. Yasuda, Solid State Ionics 132 (2000) 271–278.
[6] K. Huang, P.Y. Hou, J.B. Goodenough, Solid State Ionics 129 (2000) 237–250.
[7] Z. Yang, M.S. Walker, P. Singh, J.W. Stevenson, T. Norby, Journal of the Electrochemical Society 151 (2004) B669–B678.
[8] S.C. Paulson, V.I. Birss, Journal of the Electrochemical Society 151 (2004) A1961–A1968.
[9] J.W. Fergus, Solid State Ionics 171 (2004) 1–15.
[10] I. Yasuda, T. Hikita, Journal of the Electrochemical Society 140 (1993) 1699–1704.
[11] W.J. Weber, C.W. Griffin, J.L. Bates, Journal of the American Ceramic Society 70 (1987) 265–270.
[12] D.P. Karim, A.T. Aldred, Physical Review B 20 (1979) 2255.
[13] Y.-J. Yang, T.-L. Wen, H. Tu, D.-Q. Wang, J. Yang, Solid State Ionics 135 (2000) 475–479.
[14] N. Sakai, T. Kawada, H. Yokokawa, M. Dokiya, T. Iwata, Journal of Materials Science 25 (1990) 4531–4534.
[15] T.R. Armstrong, J.W. Stevenson, K. Hasinska, D.E. McCready, Journal of the Electrochemical Society 145 (1998) 4282–4289.
[16] L.A. Chick, J. Liu, J.W. Stevenson, T.R. Armstrong, D.E. McCready, G.D. Maupin, G.W. Coffey, C.A. Coyle, Journal of the American Ceramic Society 80 (1997) 2109–2120.
[17] J. Lambert Bates, L.A. Chick, W.J. Weber, Solid State Ionics 52 (1992) 235–242.
[18] N.M. Sammes, R. Ratnaraj, M.G. Fee, Journal of Materials Science 29 (1994) 4319–4324.
[19] H. Yokokawa, N. Sakai, T. Kawada, M. Dokiya, Journal of the Electrochemical Society 138 (1991) 1018–1027.
[20] I. Yasuda, T. Hikita, Journal of Materials Science 29 (1994) 2801–2805.
[21] T.R. Armstrong, J.W. Stevenson, L.R. Pederson, P.E. Raney, Journal of the Electrochemical Society 143 (1996) 2919–2925.
[22] M.W. Murphy, T.R. Armstrong, P.A. Smith, Journal of the American Ceramic Society 80 (1997) 165–170.
[23] N. Sakai, H. Yokokawa, T. Horita, K. Yamaji, International Journal of Applied Ceramic Technology 1 (2004) 23–30.
[24] J.D. Carter, C.C. Appel, M. Mogensen, Journal of Solid State Chemistry 122 (1996) 407–415.
[25] A. Chakraborty, R.N. Basu, H.S. Maiti, Materials Letters 45 (2000) 162–166.
[26] P. Duran, J. Tartaj, F. Capel, C. Moure, Journal of the European Ceramic Society 24 (2004) 2619–2629.
[27] M. Mori, N.M. Sammes, Solid State Ionics 146 (2002) 301–312.
[28] M. Mori, T. Yamamoto, T. Ichikawa, Y. Takeda, Solid State Ionics 148 (2002) 93–101.
[29] L. Groupp, H.U. Anderson, Journal of the American Ceramic Society 59 (1976) 449–450.
[30] L.-W. Tai, P.A. Lessing, Journal of the American Ceramic Society 74 (1991) 155–160.
[31] N. Sakai, T. Kawada, H. Yokokawa, M. Dokiya, T. Iwata, Solid State Ionics 40–41 (1990) 394–397.
[32] H. Yokokawa, N. Sakai, T. Kawada, M. Dokiya, Solid State Ionics 52 (1992) 43–56.
[33] S.W. Paulik, S. Baskaran, T.R. Armstrong, Journal of Materials Science 33 (1998) 2397–2404.
[34] T.R. Armstrong, J.W. Stevenson, D.E. McCready, S.W. Paulik, P.E. Raney, Solid State Ionics 92 (1996) 213–223.
[35] S. Wang, B. Lin, Y. Dong, D. Fang, H. Ding, X. Liu, G. Meng, Journal of Power Sources 188 (2009) 483–488.
[36] K.J. Yoon, C.N. Cramer, E.C. Thomsen, C.A. Coyle, G.W. Coffey, O.A. Marina, Journal of the Electrochemical Society 157 (2010) B856–B861.
[37] K.J. Yoon, C.N. Cramer, J.W. Stevenson, O.A. Marina, Journal of Power Sources 195 (2010) 7587–7593.
[38] K.J. Yoon, C.N. Cramer, J.W. Stevenson, O.A. Marina, Electrochemical and Solid-State Letters 13 (2010) B101–B105.
[39] L.A. Chick, L.R. Pederson, G.D. Maupin, J.L. Bates, L.E. Thomas, G.J. Exarhos, Materials Letters 10 (1990) 6–12.
[40] K. Oikawa, T. Kamiyama, T. Hashimoto, Y. Shimojyo, Y. Morii, Journal of Solid State Chemistry 154 (2000) 524–529.
[41] C.S. Montross, H. Yokokawa, M. Dokiya, L. Bekessy, Journal of the American Ceramic Society 78 (1995) 1869–1872.
[42] S. Geller, P.M. Raccah, Physical Review B 2 (1970) 1167.
[43] B. Gilbu, H. Fjellvag, A. Kjekshus, Acta Chemica Scandinavica 48 (1994) 37–45.
[44] N. Sakai, H. Fjellvâg, B.C. Hauback, Journal of Solid State Chemistry 121 (1996) 202–213.
[45] T. Hashimoto, N. Matsushita, Y. Murakami, N. Kojima, K. Yoshida, H. Tagawa, M. Dokiya, T. Kikegawa, Solid State Communications 108 (1998) 691–694.
[46] S.W. Paulik, S. Baskaran, T.R. Armstrong, Journal of Materials Science Letters 18 (1999) 819–822.
[47] V.B. Vert, J.M. Serra, J.L. Jordá, Electrochemistry Communications 12 (2010) 278–281.
[48] N.Q. Minh, Journal of the American Ceramic Society 76 (1993) 563–588.
[49] K.S. Mazdiyasni, C.T. Lynch, J.S.S. Ii, Journal of the American Ceramic Society 50 (1967) 532–537.
[50] Z. Zhong, Solid State Ionics 177 (2006) 757–764.
[51] N. Sakai, T. Kawada, H. Yokokawa, M. Dokiya, I. Kojima, Journal of the American Ceramic Society 76 (1993) 609–616.
[52] H.C. Graham, H.H. Davis, Journal of the American Ceramic Society 54 (1971) 89–93.
[53] S. Simner, J. Hardy, J. Stevenson, T. Armstrong, Journal of Materials Science Letters 19 (2000) 863–865.
[54] G.S. Lewis, A. Atkinson, B.C.H. Steele, Journal of Materials Science Letters 20 (2001) 1155–1157.
[55] D.P. Fagg, V.V. Kharton, J.R. Frade, Journal of Electroceramics 9 (2002) 199–207.
[56] R.M. German, S. Farooq, C.M. Kipphut, Materials Science and Engineering A 105–106 (1988) 215–224.
[57] S. Hayashi, K. Fukaya, H. Saito, Journal of Materials Science Letters 7 (1988) 457–458.
[58] P.S. Devi, M.S. Rao, Materials Research Bulletin 28 (1993) 1075–1082.
[59] D.-W. Kim, K.H. Ko, K.S. Hong, Journal of the American Ceramic Society 84 (2001) 1286–1290.
[60] D.-W. Kim, T.-G. Kim, K.S. Hong, Materials Research Bulletin 34 (1999) 771–781.
[61] S. Lawson, C. Gill, G.P. Dransfield, Journal of Materials Science 30 (1995) 3057–3060.
[62] S.P. Simner, J.S. Hardy, J.W. Stevenson, T.R. Armstrong, Solid State Ionics 128 (2000) 53–63.
[63] F. Boroomand, E. Wessel, H. Bausinger, K. Hilpert, Solid State Ionics 129 (2000) 251–258.
[64] P.H. Larsen, P.V. Hendriksen, M. Mogensen, Journal of Thermal Analysis and Calorimetry 49 (1997) 1263–1275.
[65] A. Zuev, L. Singheiser, K. Hilpert, Solid State Ionics 147 (2002) 1–11.
[66] R.D. Shannon, Acta Crystallographica Section A 32 (1976) 751–767.

[67] K. Hilpert, R.W. Steinbrech, F. Boroomand, E. Wessel, F. Meschke, A. Zuev, O. Teller, H. Nickel, L. Singheiser, Journal of the European Ceramic Society 23 (2003) 3009–3020.
[68] G.F. Carini, H.U. Anderson, D.M. Sparlin, M.M. Nasrallah, Solid State Ionics 49 (1991) 233–243.
[69] I. Yasuda, M. Hishinuma, Solid State Ionics 80 (1995) 141–150.
[70] S.R. Sehlin, H.U. Anderson, D.M. Sparlin, Solid State Ionics 78 (1995) 235–243.
[71] G.J. Zhang, R. Liu, Y. Yang, Y.Q. Jia, Physical Status Solidi A 160 (1997) 19–27.
[72] P.M. Raccah, J.B. Goodenough, Physical Review 155 (1967) 932.
[73] V.G. Bhide, D.S. Rajoria, G.R. Rao, C.N.R. Rao, Physical Review B 6 (1972) 1021.
[74] R. Koc, H.U. Anderson, Journal of Materials Science 27 (1992) 5477–5482.
[75] R. Koc, H.U. Anderson, Journal of the European Ceramic Society 15 (1995) 867–874.
[76] J.B. Goodenough, Physical Review 164 (1967) 785.
[77] T. Kawada, N. Sakai, H. Yokokawa, M. Dokiya, I. Anzai, Solid State Ionics 50 (1992) 189–196.
[78] T. Yamamoto, H. Itoh, M. Mori, N. Mori, T. Watanabe, N. Imanishi, Y. Takeda, O. Yamamoto, Journal of Power Sources 61 (1996) 219–222.